JACS
JOURNAL OF THE AMERICAN CHEMICAL SOCIETY
Article
pubs.acs.org/JACS

Gel-Induced Selective Crystallization of Polymorphs

Ying Diao, Kristen E. Whaley, Matthew E. Helgeson, Mahlet A. Woldeyes, Patrick S. Doyle, Allan S. Myerson, T. Alan Hatton, and Bernhardt L. Trout*

Novartis-MIT Center for Continuous Manufacturing and Department of Chemical Engineering, Massachusetts Institute of Technology, 77 Massachusetts Avenue, E19-502b, Cambridge, Massachusetts 02139, United States

ABSTRACT: Although nanoporous materials have been explored for controlling crystallization of polymorphs in recent years, polymorphism in confined environments is still poorly understood, particularly from a kinetic perspective, and the role of the local structure of the substrate has largely been neglected. Herein, we report the use of a novel material, polymer microgels with tunable microstructure, for controlling polymorph crystallization from solution and for investigating systematically the effects of nanoconfinement and interfacial interactions on polymorphic outcomes. We show that the polymer microgels can improve polymorph selectivity significantly. The polymorphic outcomes correlate strongly with the gel-induced nucleation kinetics and are very sensitive to both the polymer microstructure and the chemical composition. Further mechanistic investigations suggest that the nucleation-templating effect and the spatial confinement imposed by the polymer network may be central to achieving polymorph selectivity. We demonstrate polymer microgels as promising materials for controlling crystal polymorphism. Moreover, our results help advance the fundamental understanding of polymorph crystallization at complex interfaces, particularly in confined environments.

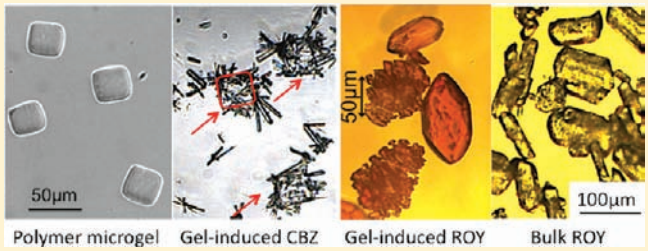

INTRODUCTION

Controlling polymorphism, the ability of a compound to self-assemble into multiple crystal structures, has been a long-standing challenge in various fields of application.[1] In particular, for pharmaceutical compounds, changes in physical properties can have a profound impact on their bioavailability and chemical stability. Crystallization involves the formation of a new phase (nucleation) and the growth of that phase (crystal growth), the mechanisms of which influence the polymorphic outcome.[2−5] Nucleation, however, is both poorly understood and poorly controlled and thus the lack of knowledge of this key process remains a major roadblock in polymorphism research.[6] One of the most challenging, yet less-explored aspects in the control of nucleation of polymorphs is the deciphering of the role of interfaces in the nucleation process, since in practice almost all nucleation events occur heterogeneously, i.e. at a foreign interface.[7] Designed nucleation substrates could be very useful in controlling polymorphism. For instance, some molecular compounds tend to crystallize in multiple polymorphs concomitantly under the same conditions.[8] By 'seeding' the solution with a designed nucleation 'catalyst' to lower the nucleation barrier of a particular polymorph selectively, controlled polymorph nucleation can potentially be achieved.

Several types of substrates have been studied for screening or controlling polymorphs of molecular crystals, including crystalline substrates,[9] two-dimensional (2D) ordered surfaces such as self-assembled monolayers[10−12] and insoluble polymer surfaces.[13] On these flat and smooth substrates, polymorph selectivity seems to be best achieved when both lattice matching (epitaxy) and complementary chemical interactions at the crystal−substrate interface are satisfied.[10,14] In recent years, materials imposing a nanoscopically confined environment for crystallization have also been explored for polymorph control, such as controlled pore glass with pores ranging from a few to a hundred nanometers[15−17] and microemulsions with drop sizes of 2−10 nm.[18,19] Stabilization of metastable polymorphs in sufficiently small nanoconfined domains was often observed,[15,17] but not always.[18,19] To explain these observations, evidence was presented that the large surface area to volume ratio can alter the relative polymorph stability.[16] Another hypothesis frequently evoked states that when the pore size becomes smaller than the critical nucleus size of a polymorph, crystallization of this polymorph is hindered in confinement.[15] However, these arguments fail to account for the nucleation-templating effect of the confining interfaces. Moreover, the kinetic aspects of polymorph control under nanoconfinement have been ignored, even though kinetics plays the governing role in polymorphic outcomes.[6] In fact, systematic studies on the kinetics of polymorph nucleation have rarely been reported in general, not only in the nanoconfinement literature.

Here, we report the use of a novel material, polymer microgels,[20] for understanding and controlling polymorph crystallization of molecular compounds in a confined environment. The microgels exhibit a meshlike structure, formed by cross-linking polyethylene glycol diacrylate (PEGDA) of

Received: October 24, 2011
Published: December 3, 2011

   dx.doi.org/10.1021/ja210006t | J. Am. Chem.Soc. 2012, 134, 673−684

varying PEG subchain molecular weight M (g/mol). When immersed in solution, the microgel swells by taking up solute and solvent molecules owing to favorable interactions, and the degree of swelling, which varies depending on the PEG subchain length, defines the average gel mesh size, a quantity typically used for describing the microstructure of the swollen polymer network.[21] With mesh sizes ranging from a few angstroms to several nanometers, the polymer network partitions the absorbed solution and restricts the mobility of adsorbed solute molecules,[20,22] thereby providing a confined environment for crystallization to take place.

Using polymer microgels of tunable mesh size, we investigate systematically the nanoconfinement effect on polymorphism with two model compounds, carbamazepine (CBZ) and 5-methyl-2-[(2-nitrophenyl)amino]-3-thiophenecarbonitrile (ROY). We find that their polymorphic outcomes are strongly dependent on the polymer mesh size and chemical composition. In addition, there exists an evident correlation between nucleation kinetics and polymorphic outcome. We examine the underlying mechanisms from three aspects: the influence of mesh size, preferential partitioning and specific polymer-solute interactions. We further propose that the selectivity of polymorph nucleation arises from the templating effect driven by specific polymer-solute interactions, which, facilitated by an optimum spatial configuration imposed by the confinement effect, enhance the nucleation of a particular polymorph to the greatest extent.

RESULTS AND DISCUSSION

Monodispersed cubelike PEGDA microgels (Figure 1 left), with M ranging from 130 to 700 g/mol were synthesized by stop-flow lithography[23] following a procedure described in our previous work.[20] Their mesh sizes vary from 0.7 to 1.5 nm in solvent ethanol (Table 1), estimated from equilibrium swelling by the Flory–Rehner theory.[20,24] The accuracy of this method for obtaining mesh sizes has been confirmed using small-angle neutron scattering in a different solvent.[22] The microgels were utilized for controlling polymorph crystallization by suspending ~10 μg of microgels per 1 mL solution with stirring. Such a low microgel concentration is already sufficient to effect drastic changes in crystallization behavior (as discussed later), underscoring the effectiveness of polymer microgels in controlling crystallization. In all crystallization experiments, supersaturation of the solution was generated by cooling instead of solvent evaporation, which has been used frequently in numerous polymorph studies, to yield better control over the crystallization process.

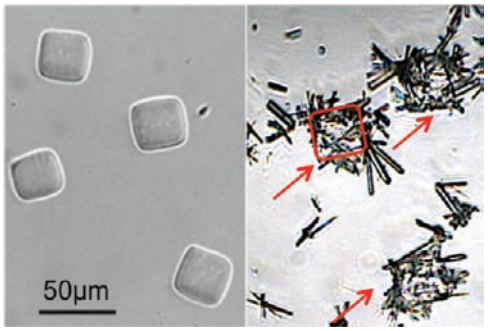

Figure 1. Optical micrographs of $PEG_{400}DA$ microgels as synthesized (left) and CBZ form II needles grown on $PEG_{400}DA$ (right), in which three microgels covered with CBZ needles are indicated with red arrows, and the contour of the middle one is traced with a red line to delineate the cubic gel.

We selected CBZ and ROY as model compounds to represent both packing polymorphism (CBZ) and conformational polymorphism (ROY), where CBZ polymorphs have the same conformer arranged in differing molecular packing motifs[25] and ROY polymorphs, in comparison, assume distinctive molecular conformations in various packing arrangements, with altered conjugation state and thus different colors between different polymorphs.[26] Both molecules have been studied extensively for purposes of polymorph screening[12,13] and control.[15] CBZ possesses four known anhydrous forms, and ROY has ten known forms with seven structurally characterized. The complexity of the two systems poses challenges for their polymorph control. Specifically, concomitant crystallization (simultaneous crystallization of multiple forms in the same liquid),[8] has been reported for both systems.[27−30] In addition, crystallization of ROY polymorphs also suffers from poor reproducibility[29] owing to the stochastic nature of the process.[12]

Crystallization of CBZ Polymorphs Induced by Microgels. Out of the four known anhydrous forms of CBZ, triclinic form I, trigonal form II, primitive monoclinic form III and C-centered monoclinic form IV, form III is the most stable under ambient conditions, followed by forms I, IV, and II, with the energy separation between forms III and II less than 0.7 kcal/mol.[25] Such a narrow energy window suggests that the CBZ polymorph crystallization is very sensitive to experimental parameters. Not surprisingly, there have been some inconsistencies in previous reports on the CBZ polymorphic outcome during crystallization from solution under similar conditions. For instance, when crystallized from highly supersaturated ethanol solution (often with supersaturation $S > 3$) by cooling to low temperatures ($T < 10$ °C), Grzesiak et al[25] obtained pure form II; Nokhodchi et al[31] crystallized pure form III; Getsoian et al[32] reported pure form II, although it in

Table 1. Effect of PEGDA Microgels on the Average Nucleation Induction Time and Polymorphic Outcome for CBZ[a]

M (g/mol)	bulk	130	200	400	575	700
ξ (nm)	NA	0.7	0.8	1.1	1.3	1.5
polymorph	**II** and **I**, occasionally **III**	**II** and **I**	**II** and **I**	**II**	**II**	**II**
τ (min)	427 ± 13	222 ± 5	174 ± 11	10.9 ± 0.3	33 ± 1	49 ± 1
β	0.86	0.99	0.73	1.00	0.61	0.94
R^2	0.986	0.982	0.960	0.976	0.981	0.987

[a]Average mesh size ξ was estimated from equilibrium swelling experiments[20] in solvent ethanol. Polymorphic outcomes were analyzed by XRD (Figure 2). Induction time distribution data were fit with stretched exponentials via nonlinear least square regression: $P = \exp[-(t/\tau)^{\beta}]$, where P is the probability of observing no crystallization event within time t, τ is the average induction time, and β is the stretched exponential exponent.

fact seems to be a mixture of forms I and II, judging from their XRD results. At a lower supersaturation (S = 2) and higher temperature (T = 25 °C), concomitant crystallization of forms II and III was observed by Kelly et al,[27] also from ethanol solution. In this study, we found that CBZ crystallization is quite sensitive to experimental conditions such as impurity concentration, solution water content (trace amount), stirring speed, etc., which could explain some of the aforementioned inconsistencies (see Experimental Methods). Therefore, all crystallization conditions were strictly controlled in this study to ensure reproducible results.

Under the experimental conditions employed in this work (S = 1.63, T = 25 °C, 2 mL of purified solution stirred at 300 rpm), concomitant crystallization of forms I and II, both with needlelike crystal habits, was observed consistently (~100 trials) when crystallized from the bulk ethanol solution (Table 1, Figure 2), Occasionally, pure form III was also obtained,

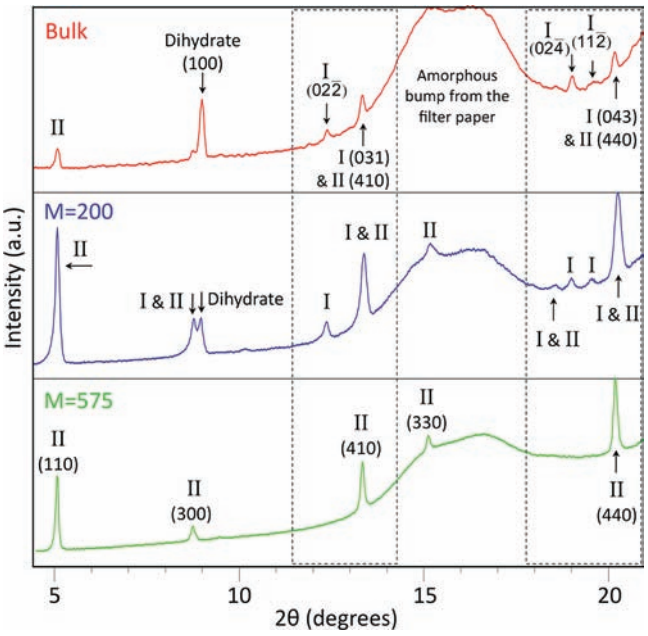

Figure 2. X-ray diffraction patterns of CBZ from bulk solution (top) and in the presence of PEGDA microgels, for which representative patterns are shown for M = 200 (middle) and 575 (bottom) g/mol. CBZ forms I and II peaks are labeled with miller indexes (hkl) in the top and bottom panels, respectively. The regions where major characteristic peaks of form I reside are outlined with black dotted lines. The hump between 12 and 20° is from the filter paper, since the crystals (harvested as soon as the crystallization ensued) were too few to be scraped off from the filter paper. A peak at 9.00° appears in some patterns, corresponding to CBZ dihydrate which forms during filtration, especially when the ambient humidity is high. This explanation is corroborated by control experiments where clear CBZ solution was passed through the filter paper, the XRD scan of which only revealed the dihydrate peak.

which may be due to the stochastic nature of polymorph crystallization, where form III has a high kinetic barrier to nucleation and thus a low frequency of occurrence under the experimental conditions. The possibility of observing both I and II forms due to the solvent-mediated polymorph transformation was eliminated because the crystal mixtures, which were sampled at intervals and characterized by XRD, did not exhibit statistically significant changes in polymorphic composition during the aging in solution following the onset of nucleation, Interestingly, when PEGDA microgels with $M \geq$ 400 g/mol were added to the solution, pure form II as identified by XRD (Figure 2) crystallized (~250 trials), whose needle-shaped crystals were observed to grow from the microgel surface (Figure 1 right). However, such polymorph selectivity could not be attained using microgels with M < 400 g/mol (~100 trials) where the polymorphic outcome was quite similar to that of the bulk samples (Table 1), only with a decreased mass fraction of form I obtained in the mixture (Figure 2) and a lower frequency of occurrence of form III.

Accompanying the impact on CBZ polymorphic outcomes is the ability of the microgels to alter the CBZ nucleation kinetics, characterized by the average nucleation induction time τ (Table 1). Induction time was measured by monitoring the IR transmission signal passing through a stirred solution under controlled temperature conditions. Once nucleation occurs, the solution becomes turbid in seconds indicated by a sharp drop in the IR signal, due to secondary nucleation and rapid crystal growth. The statistical nature of nucleation necessitates a large number of experiments (50−100) to obtain the distribution of induction times, from which the average induction time τ is extracted using a stretched-exponential model, $P(t) = \exp[-(t/\tau)^{\beta}]$,[22] where P is the probability of observing no crystallization event within time t, estimated from the fraction of samples not crystallized within time t. The stretched-exponential model modifies the single exponential model derived from the Poisson statistics,[33] $P(t) = \exp(-t/\tau)$, by raising the dimensionless induction time t/τ to the power of β to capture the spread in characteristic time scales. The spread of nucleation time scales could be caused by a distribution of nucleation active sites present in the system, and/or by the existence of multiple nucleation pathways.[34,35] In the gel-containing solution under investigation, a distribution of nucleation sites may arise from the spatial variations in both the mesh size and the chemical composition of the microgels, as discussed in our previous study.[22] Such structrual charateristics of the microgel are described as quenched disorder in statistical physics terms. The microgel is 'disordered' since the polymer network is generated by random cross-linking, and this disorder is quenched in the sense that the structure does not evolve with time. Therefore, microgel-induced nucleation serves as an example of first-order phase transformation in the presence of quenched disorder, common examples of which are nucleation induced by uncontrolled impurities[36] or rough vessel surfaces.

Shown in Table 1 and Figure 3, microgels with M = 130 and 200 g/mol effectively shortened the CBZ average induction times by 2−3-fold relative to those of the bulk samples, whereas at least an order of magnitude reduction was observed with microgels of higher M. More importantly, there exists a strong correlation between the extent of nucleation acceleration and the polymorph selectivity, wherein form II was obtained exclusively only with those microgels that were sufficiently effective in promoting nucleation. Since form II is the least stable polymorph under ambient conditions, this correlation leads us to the hypothesis that the observed polymorph selectivity toward a higher-energy form may be driven by kinetic factors, in which case the presence of microgels preferentially lowers the kinetic barrier to form II nucleation, as opposed to switching the relative stability between I and II.

Mechanistic Investigations into CBZ Polymorph Selectivity. The microgels altered the relative nucleation rates of CBZ polymorphs through various means. First, we investigated the 'concentration effect' on the basis of the

dx.doi.org/10.1021/ja210006t | J. Am. Chem.Soc. 2012, 134, 673−684

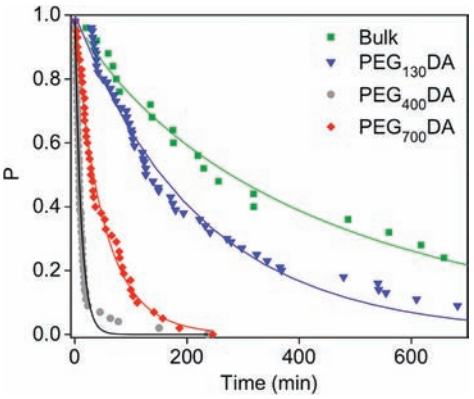

Figure 3. Nucleation induction time statistics for CBZ in the presence and absence of PEGDA microgels. *P* is the probability of observing no crystallization event within time *t*. The stretched exponential model was employed to fit the data (see Table 1), and the fitted curves are displayed as solid lines. Data obtained with $PEG_{200}DA$ and $PEG_{575}DA$ are omitted for clarity.

knowledge that the microgels have the ability to concentrate solute molecules via favorable polymer−solute interactions.[20] A higher local density of solute may enhance effective solute−solute interactions and thereby facilitates molecular cluster formation, although the higher solute concentration in the gel does not necessarily increase the supersaturation as the chemical potential of the solute in the bulk and the gel must be equal at equilibrium. Equilibrium partitioning experiments revealed that the CBZ concentration in the polymer gel is 3−4 times higher than that in the bulk (Figure 4). In addition, a

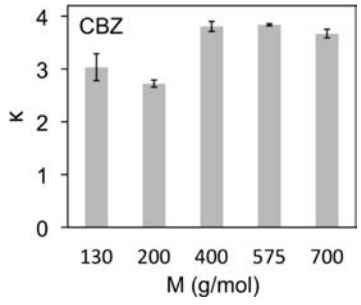

Figure 4. Partition coefficients (κ) of CBZ in PEGDA microgels with respect to ethanol solutions. κ is defined as the ratio of solute mass fraction in the solution confined in the gel to that in the bulk. The error bars are calculated from three to four independent repeats.

generally higher partition coefficient κ in microgels with larger *M* suggests that CBZ prefers interacting with the PEG rather than with the acrylate segments. To assess the effect of solute concentration on polymorphic outcomes, bulk crystallization experiments were conducted at a series of starting concentrations, and the resultant form I and II mixtures were analyzed with XRD to quantify the polymorph compositions. As shown in Figure 5, an increasing solute concentration results in a reduced form I mass fraction and thus biases the polymorphic outcome toward the less stable form II. This trend is not unexpected since in practice less stable forms are typically generated by increasing the supersaturations to drive the system toward the kinetic control regime. However, using this strategy we could not eliminate form I to obtain pure form II, even at concentrations as high as 140 mg/mL (S = 6.7). In fact, when the concentration increased beyond 60 mg/mL, the polymorph

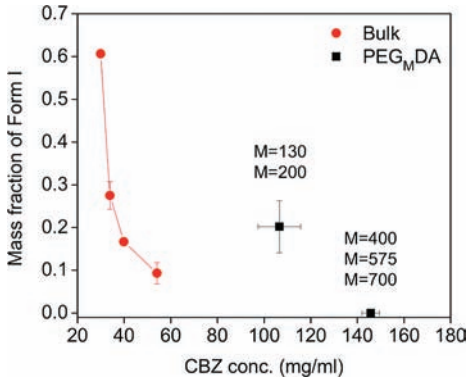

Figure 5. Effect of solute concentration on the polymorphic composition of CBZ crystals. For samples with PEGDA microgels, the *X*-axis corresponds to the effective solute concentration of solution inside the gel, calculated by multiplying the solute partition coefficient (Figure 4) by the bulk concentration, 34 mg/mL, for all samples with microgels. The *X* error bars are from partition coefficient measurements, and the *Y* error bars are calculated from XRD measurements on three independent samples. The method for quantifying the mass fraction of form I is detailed in the Experimental Methods section.

composition became irreproducible since, before the solution was cooled to the desired supersaturation level, crystallization had already ensued. In contrast, the microgels can take the system into a parameter space inaccessible through conventional means. For samples with microgels, we observed the same trend as seen with the bulk samples (Figure 5), which indicates that higher solute concentrations in the gel could facilitate selective nucleation of form II. Yet, the high degree of selectivity cannot be explained quantitatively in terms of only the concentration effect, which prompted us to examine other contributing factors, such as the nucleation templating effect of the PEGDA polymer.

Besides increasing the solute concentration in the gel, favorable polymer−solute interactions can also induce a 'templating effect', by which the CBZ molecules are directed toward a particular orientation via molecular interactions and thereby the entropic cost of nucleus formation is reduced. This microscopic phenomenon should be expressed macroscopically as the preferred orientation of crystals on flat polymer surfaces, which can be detected via XRD.[22,33] The methodology is described in the Experimental Methods section. We indeed observed a preferred crystal orientation and, specifically, the PEGDA polymer surface induced nucleation of a particular set of crystal planes of form II only, i.e., (110) and its higher index planes, irrespective of the PEG subchain molecular weight (Figure 6a). Such high specificity is remarkable, considering that the surface of the cross-linked polymer is 'disordered', in contrast to 2D crystalline surfaces utilized extensively for inducing highly specific crystal orientation by the epitaxy mechanism.[37] This observation suggests the importance of interfacial interactions in directing the nucleation process and provides strong evidence for the templating effect as a critical contributing factor to the microgel-induced polymorph selectivity.

To identify the specific polymer−CBZ interaction responsible for directing form II nucleation, the surface chemistries of II (110) and II (440) were compared with those of other major crystal facets not nucleated from the polymer surfaces, namely, II (410), I ($02\bar{2}$), and I ($02\bar{4}$) (Figure 2; note that the XRD patterns in Figure 2 were obtained with randomly oriented

dx.doi.org/10.1021/ja210006t | J. Am. Chem.Soc. 2012, 134, 673−684

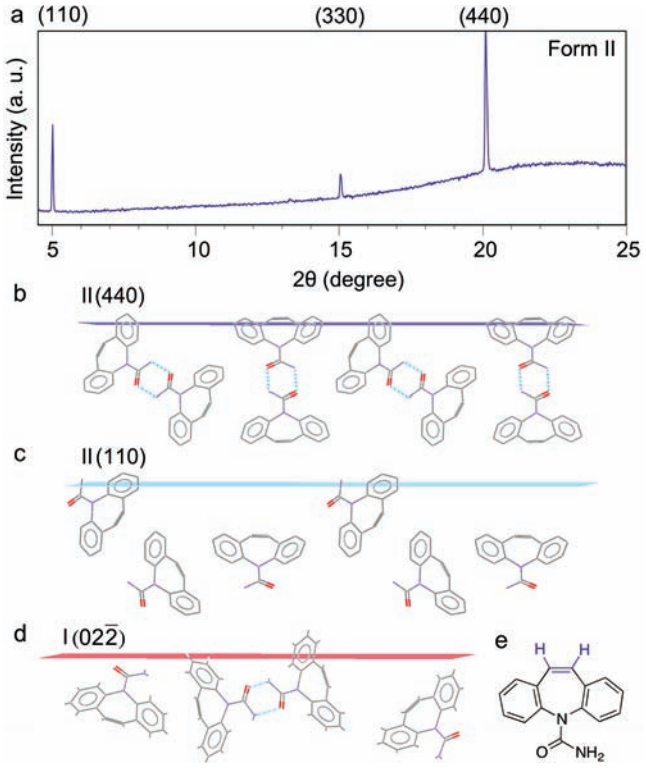

Figure 6. Specific CBZ–polymer interactions inferred from preferred crystal orientations. (a) XRD pattern of CBZ crystals grown on PEGDA films. Relative peak intensities were found to be independent of *M*. A representative pattern is shown. (b, c) Surface structures of form II facets preferentially nucleated on polymer surfaces. (d) Surface structure of a facet characteristic of form I not grown from polymer surface. (e) Functionality inferred to interact preferentially with PEGDA polymer (colored blue).

crystal powders and therefore capture a statistical average of all crystal facets grown from the system). All II (410), I (02$\bar{2}$), and I (02$\bar{4}$) facets exhibit similar surface chemistries, dominated by the phenyl group on the azepine ring and decorated with the carboxamide group (Figure 6d; only I (02$\bar{2}$) is shown). In comparison, the vinyl group is a distinctive functionality characterizing the II (440) facet. This analysis implies that it is the vinyl group of CBZ that is mainly engaged in its interaction with PEGDA (Figure 6e), possibly by forming the C–H···O contact[38] between the vinylic hydrogen of CBZ and the oxygen of the PEG subchain. Albeit weak, such interactions have been found to play an important role in directing nucleation processes[10,22] and in distinguishing polymorphs of many organic crystals.[38]

In summary, both the concentration effect and the templating effect are found likely to contribute to the observed CBZ polymorph selectivity induced by polymer gels. Considering the striking similarity of the intermolecular interactions between forms I and II of CBZ,[25] the polymorph selectivity achieved with the microgels is indeed remarkable. It is also worth noting that the CBZ polymorphic outcomes seem to be quite sensitive to the polymer mesh sizes, with exclusive nucleation of form II only obtained using microgels of larger mesh sizes, the implication of which is discussed later and summarized as the 'mesh size effect'.

Crystallization of ROY Polymorphs Induced by Microgels. ROY crystallization is well-known for its poor polymorph selectivity for two reasons. First, when crystallized from solution, multiple polymorphs can be obtained (often in pure forms, occasionally concomitant) from the same solution under seemingly identical conditions.[12,29,30] Second, during crystallization from supercooled melts, concomitant polymorphs are frequently observed, controlled by both the nucleation and crystal growth kinetics.[4] Here we are interested in solution crystallization, where the poor selectivity may arise from a broad distribution of molecular conformations in solution, in addition to the small free energy differences between ROY polymorphs as in the case of CBZ.[29]

In each experiment, we observed crystallization of pure forms of either Y (yellow prisms), R (red prisms), or ON (orange needles) from ethanol solution to occur stochastically (Figure 7), and their frequencies of occurrence were calculated by conducting 50–150 experiments in each case (Figure 9). Nucleation induction time data from bulk solution or with PEG$_{130}$DA microgels were fitted with the stretched exponential model, and the average induction time thus regressed represents an average over all forms (Figure 8a, Table 2), since the frequencies of occurrence for R and ON were too low for separate statistical analysis. Low values of the stretched exponential exponent β (Table 2) indicate a wide spread of nucleation time scales, the exact reason for which is unclear. We

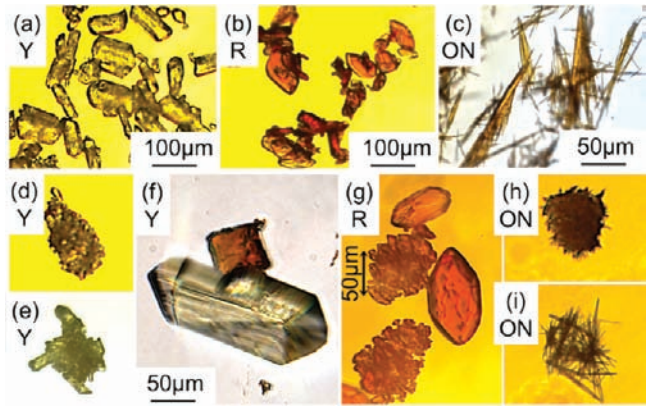

Figure 7. Optical micrographs of ROY crystallized from (a–c) bulk and on (d–i) microgels, specifically, with *M* = 400, 575, 700, 400, 400, 400 g/mol in images d, e, f, g, h, i, respectively. Y, R, and ON denote yellow prism, red prism, and orange needle forms, respectively. Scale bars for images (d–i) are the same as shown in (f). In images (d, e, g, h, i), the cubic microgels are covered with tiny ROY crystals grown from their surfaces, whereas in image (f), only one, large, single crystal nucleated on the gel, leaving the red-colored microgel clearly visible. The originally transparent microgel became red in solution due to high preferential partitioning of ROY into the gel (Figure 10) or polymer–solute interaction-induced conformation change.

Table 2. Average Nucleation Induction Times of ROY in Bulk and with PEG$_{130}$DA Microgels[a]

samples	τ, min	β	R^2
bulk	10000 ± 2000	0.37 ± 0.02	0.97
PEG$_{130}$DA	4000 ± 750	0.25 ± 0.01	0.97

[a]Induction time distribution data were fitted with stretched exponentials via nonlinear least-squares regression: $P = \exp[-(t/\tau)^{\beta}]$, where P is the probability to observe no crystallization event within time t. τ is an average of the induction times for all Y, R, and ON forms.

dx.doi.org/10.1021/ja210006t | J. Am. Chem.Soc. 2012, 134, 673–684

Table 3. Average Nucleation Induction Times of ROY with PEGDA Microgels, (M = 200−700 g/mol)[a]

microgels	τ(Y), min	τ(R), min	τ(O), min	a	b	R^2
$PEG_{200}DA$	26.0 ± 1.5	9000 ± 6000	NA	0.550	NA	0.983
$PEG_{400}DA$	22.0 ± 0.6	1600 ± 400	3300 ± 1200	0.298	0.330	0.995
$PEG_{575}DA$	10.0 ± 0.8	200 ± 20	2900 ± 500	0.205	0.350	0.996
$PEG_{700}DA$	12.0 ± 1.2	2600 ± 400*		0.375	NA	0.967

[a]Induction time distribution data were fitted with superposition of two or three exponentials via nonlinear least squares regression. Two-exponential fits were employed for the $PEG_{200}DA$ and $PEG_{700}DA$ samples: $P = a\exp[-t/\tau(Y)] + (1-a)\cdot\exp[-t/\tau(R)]$, with $\tau(R)$ an average of forms R and O for the $PEG_{700}DA$ sample. A three-exponential fit was used for the $PEG_{400}DA$ and $PEG_{575}DA$ samples: $P = a\cdot\exp[-t/\tau(Y)] + b\cdot\exp[-t/\tau(R)] + (1-a-b)\cdot\exp[-t/\tau(O)]$, where Y, R, and O represent the yellow, red, and orange needle forms respectively. *τ is an average induction time of forms R and ON, given the lack of data points to distinguish the two.

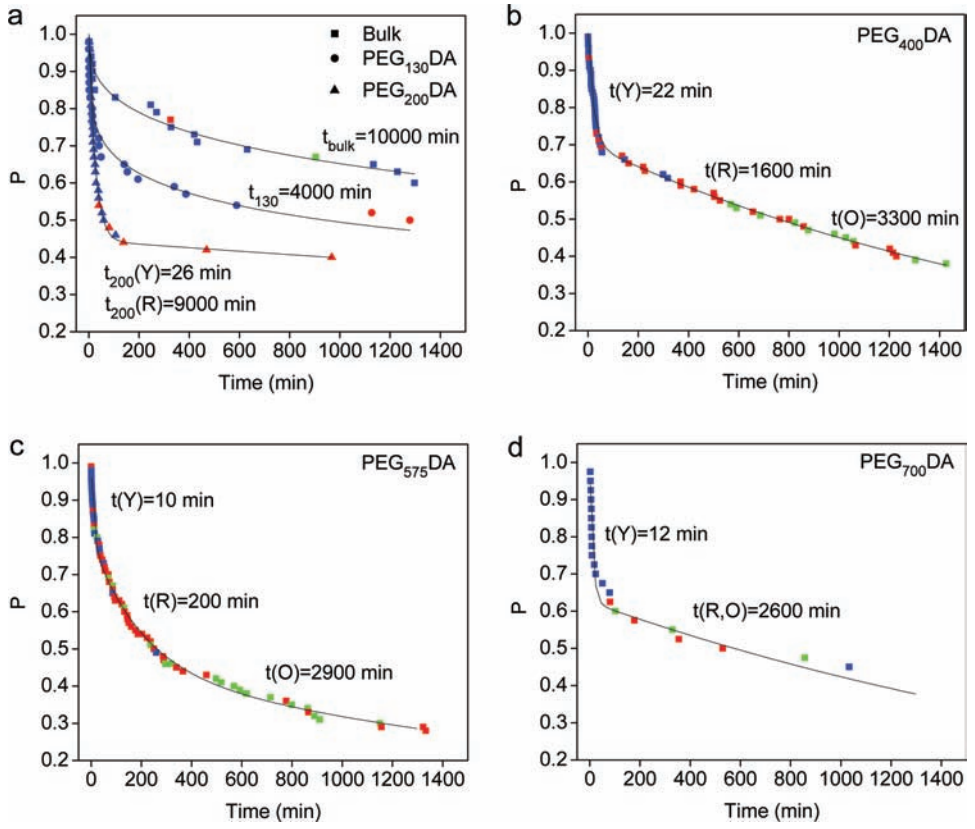

Figure 8. Nucleation induction time statistics of ROY in the absence and the presence of PEGDA microgels. Each data point corresponds to one individual crystallization experiment. A data point is colored blue, red, or green to indicate which of the forms Y, R, or ON was obtained in this experiment. For each type of sample, 50−100 experiments were performed to obtain the induction time statistics. P, the probability for observing no crystallization event within time t is estimated from the fraction of samples that had not crystallized at that time point. Either the stretched exponential model or the multiexponential model was employed to fit the data (see Tables 2 and 3), and the fitted curve is displayed as a black solid line. Each exponential decay process is labeled with its characteristic time scale obtained from the model fitting.

speculate that it could be associated with a broad conformation distribution of ROY in solution since such low β values have not been observed with systems exhibiting packing polymorphism, such as carbamazepine, aspirin and acetaminophen.[22] The validity of this explanation would require that the rate of achieving conformational equilibrium is slow relative to the rate of nucleation. Induction time data obtained with microgels of M = 200−700 g/mol can be described very well with multiexponential models (Figure 8, Table 3), with each exponential decay process corresponding to a particular polymorph, and the characteristic decay time of each exponential being the average nucleation induction time of the corresponding polymorph.[39] In the multiexponential model, each exponential decay process may be better represented by a stretched exponential to take into account the quenched disorder phenomena discussed above. However, a simple exponential was found to suffice in this case, and good fits were obtained with R^2 very close to unity (Table 3). This is probably because, when the time scales corresponding to different polymorphs are at least an order of magnitude apart, the effect of quenched disorder on the nucleation of each polymorph becomes secondary in comparison.

For bulk crystallization without microgels, we observed predominantly form Y under the chosen experimental conditions (see Experimental Methods) and occasionally forms R and ON (Figure 7 a−c, Figure 8a, Figure 9 left). The relative stabilities of the three observed polymorphs are in the order Y > ON > R under these conditions. Our observation is consistent with previous reports, such as that by Alvarez who obtained primarily Y from various supercooled solutions.[40] The

dx.doi.org/10.1021/ja210006t | J. Am. Chem.Soc. 2012, 134, 673−684

addition of microgels had a great impact on ROY nucleation kinetics and polymorph frequency of occurrence, the extent to which varied considerably with the polymer mesh size. Shown in Figure 8a and Table 2, $PEG_{130}DA$ microgels expedited nucleation of the Y form, but its effect on crystallization of other forms was not very pronounced. When $PEG_{200}DA$ microgels were injected into the ROY solution, nucleation of Y was further accelerated, all of which occurred within 100 min, and form R also began to appear at a detectable rate. Naturally, the observed promotion of Y and R nucleation kinetics was reflected in increased frequencies of occurrence for both forms (Figure 9 left). With the addition of PEGDA gels of larger mesh sizes (Figure 8b–d, Table 3), form ON nucleation was accelerated into the detectable range as well, but its average rate was much slower than the rates of forms Y and R in all cases. Meanwhile, nucleation of form R continued to be promoted with increasing M, and a maximum nucleation rate was attained with $PEG_{575}DA$ microgels, for which the average induction time of R was reduced to 200 min from well over 10000 min in the absence of microgels. Correspondingly, the frequency of occurrence for R also peaked at M = 575 g/mol, replacing Y as the dominant polymorph (Figure 9 left). Evidence of ROY polymorphs nucleated on microgels is shown in Figure 7 d–i.

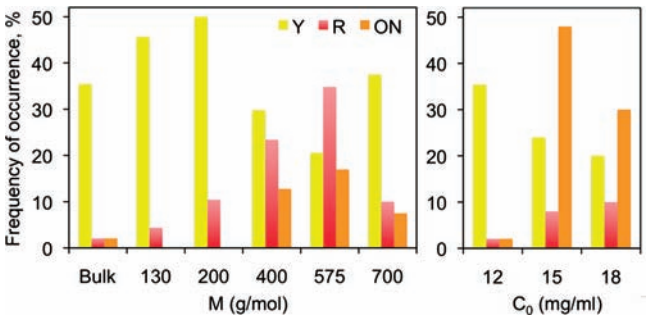

Figure 9. Polymorph frequency of occurrence in 12 mg/mL ROY–ethanol solutions with or without microgels of various mesh sizes (left) and at higher solution concentrations, C_0 (right). Frequency of occurrence is calculated as the percentage of samples crystallized in a particular form within 1440 min out of the total number of samples. The analysis for 12 mg/mL solution is carried out on the data set the same as that in Figure 8.

Notably, previous researchers found that the frequency of occurrence of form R was quite low compared with that for forms Y and ON during solution crystallization from various solvents,[12,30,40] particularly when supersaturation was achieved by cooling as in this study. Alvarez[40] showed that the R polymorph was obtained only once out of 42 experiments despite the use of multiple solvents and cooling rates. Hilden[30] also obtained predominantly forms Y and ON by evaporating ethanol in capillaries. Though other methods have been used for screening rare ROY polymorphs,[13] the reproducibility and selectivity were not reported. In this study, we demonstrate that addition of polymer microgels improved the frequency of occurrence of form R by up to 20 times even at relatively low supersaturation, an effect not easily attainable by conventional means.

In summary, addition of PEGDA microgels accelerated crystallization of all three forms, Y, R, and ON. Particularly, nucleation of a metastable form R was induced preferentially to become the dominant form at an optimum mesh size M = 575 g/mol, whereas Y crystallized almost exclusively in the absence of microgels. Nucleation of another metastable form, ON, was also promoted when M > 200 g/mol, however, to a much lower extent than for R. Interestingly, ROY nucleation kinetics is extraordinarily sensitive to the variation in mesh sizes, particularly for form R.

Mechanistic Investigations of ROY Polymorph Selectivity. The impact of microgels on ROY polymorphic outcome can be comprehended from the perspectives of the concentration effect, the templating effect, and the mesh size effect. Similar to CBZ, ROY also exhibits preferential partitioning to the gel phase (Figure 10), which leads to concentrations 6–11 times higher than those of the bulk solution. This result is visibly reflected in the red color of the microgels (Figure 7f) imparted by the highly concentrated ROY. In addition, the fact that κ is much higher at larger M indicates ROY interacts predominantly with the PEG subchain. The influence of higher solute concentrations on polymorphic outcomes was investigated with bulk crystallization experiments (Figure 9 right). Clearly, ON became the dominant form with the increase in concentration, which is in accordance with previous reports.[30] This concentration effect could help explain the accelerated nucleation of ON when microgels with M = 400–700 g/mol were added (Figure 9 left), considering that the ROY concentration in these microgels is much higher than in others (Figure 10). Apparently, the concentration effect cannot fully account for the observation that crystallization of the R form was particularly promoted by microgels. The strong dependence of form R nucleation kinetics and frequency of occurrence on M suggests that the mesh size effect and the ROY–polymer interactions may play key roles in controlling R form nucleation.

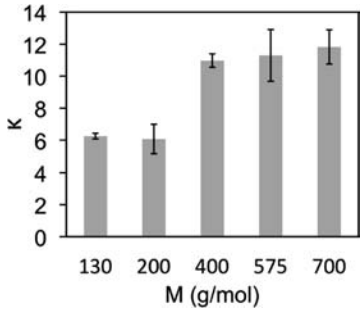

Figure 10. Partition coefficients of ROY in PEGDA microgels from ethanol solution.

The ROY–polymer interactions were probed via preferred crystal orientations on flat PEGDA films. The polymer films were synthesized using the same formulation as that of microgels, but without the presence of porogen and solvent so as to diminish the impact of varying microstructures and to focus on the effect of specific interactions. From the bulk solution, ROY crystallized in form Y predominantly (Figure 11). In comparison, PEGDA films templated nucleation of R, as well as Y, which is consistent with the observations with microgels. In particular, a few crystal facets show much stronger XRD peak intensities compared with those in the bulk sample, i.e., Y (020), R (111), and R (220), indicating that they are the dominant crystal facets nucleated on the polymer. To verify this observation, we quantified the contribution from each crystal facet and listed the prominent ones in Table 4. Interestingly, the preferred crystal orientation varies significantly as a function

dx.doi.org/10.1021/ja210006t | J. Am. Chem.Soc. 2012, 134, 673–684

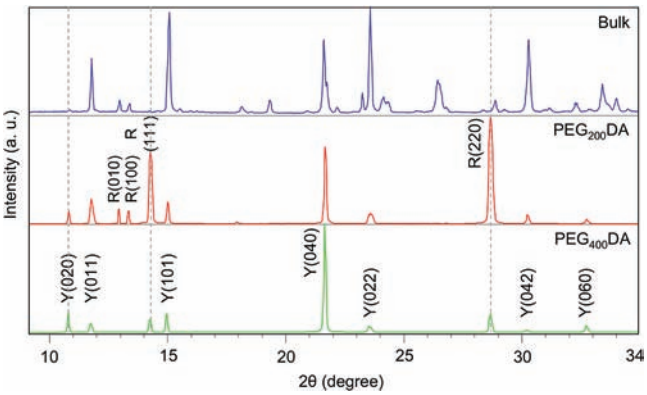

Figure 11. XRD patterns of ROY crystallized from bulk solution (top) and on PEGDA films (middle and bottom) under the same conditions. Additional peaks observed from crystals templated by polymer films but not from bulk crystals are marked with vertical gray dotted lines. Reference patterns are calculated from CSD using POWD-12++.

Table 4. Percentages of ROY Crystals in Various Orientations (*hkl*) on PEGDA Polymer Films[a]

M (g/mol)	Y (020), %	Y (040), %	R (111), %	R (220), %
130	7.5	3.4	**38.0**	**46.8**
200	3.5	1.6	**36.2**	**53.6**
400	**23.6**	9.9	**28.8**	**24.9**
575	**26.9**	13.1	12.9	20.0
700	**50.9**	16.9	9.8	14.4

[a]The quantification method is described in the Experimental Methods section. Minor orientations (<10% on all films) are considered but not shown in the table. Percentages are highlighted as bold for dominant orientations in each case.

of *M*, the PEG subchain molecular weight. Polymers with *M* = 130, 200 g/mol favor R (111) and R (220). As *M* increases, the percentage of R decreases and that of Y increases to become the dominant polymorph for *M* = 575, 700 g/mol, which is in contact with the polymer via the Y (020) and/or (040) facets. This observation implies that the acrylate group of PEGDA is responsible for templating R, whereas the PEG subchain induces nucleation of Y. Furthermore, it underscores the point that the polymorph crystallization is extraordinarily sensitive to polymer–solute interactions.

To unveil the specific polymer–solute interactions, we examined the molecular structures of preferentially nucleated crystal facets, shown in Figure 12. R (111) and R (220) exhibit very similar surface functionalities. The cyano and nitro moieties, although exposed to the surface, are engaged in ROY self-interactions, leaving the amine and methyl groups more available to interact with the polymer surface (Figure 12d), probably with the acrylate group as inferred from the XRD results (Table 4). Specifically, the amine hydrogen of ROY can form a hydrogen bond with the carbonyl of the acrylate group, and the methyl group of ROY can interact with acrylate by forming a C–H···O contact, which is often referred to as a secondary hydrogen bond in the crystal engineering literature.[38] As for form Y, either Y (020) or Y (040) or both were possibly templated by the polymer; they cannot be distinguished from the XRD spectra since they are parallel planes. However, it is unlikely for Y (040) to interact directly with PEGDA, because it resembles Y (022) and Y (042) in surface chemistry (not shown), neither of which is favored by the polymer, although both are among the main facets of bulk

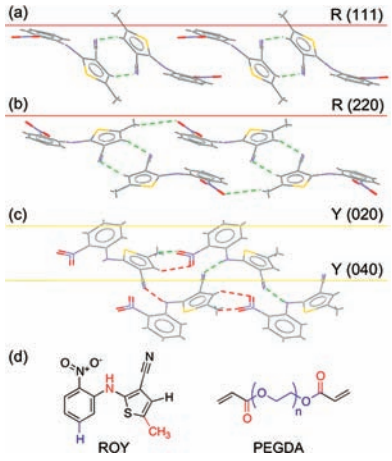

Figure 12. Specific polymer–ROY interactions inferred from preferred crystal orientations. (a–c) Molecular structures of ROY crystal facets preferentially grown from the polymer surface. The solid line indicates the top surface of the corresponding facet. R and Y denote red and yellow ROY polymorphs. Prominent intermolecular interactions in ROY crystals are denoted with green dotted lines if the interaction is between the two in-plane molecules as depicted, and with red dotted lines if it is between one in-plane molecule and another molecule in the next layer in the through-plane direction. (d) Molecular structures of monomers of ROY and PEGDA. ROY functional groups colored blue are inferred to interact preferentially with the PEG subchain, and those colored red with the acrylate group.

crystals (Figure 11). All Y (022), (042), and (040) facets are featured with cyano and/or nitro moieties, which are more likely to engage in ROY intermolecular interactions or solvated by ethanol. Therefore, the phenolic hydrogen exposed to the Y (020) surface is inferred to be responsible for interacting with the PEG subchain (Figure 12d), probably by forming a C–H···O contact with the ethylene oxide oxygen.

The identified specific ROY–polymer interactions can help elucidate the role of the templating effect in polymorph selection. By interacting with the phenolic hydrogen of ROY, the PEG subchain brings about two effects. First, it helps align the ROY molecules in a particular orientation and, as such, better exposes other moieties in ROY for self-interactions and facilitates molecular cluster formation, which is a key step to nucleation. Second, it hinders the phenolic hydrogen-nitro recognition essential to R polymorph formation (not found in other forms with known structures except for OPR) (Figure 13 c,d), resulting in preferential nucleation of the Y polymorph on polymer films with higher *M*. Likewise, by hydrogen bonding with the amine moiety of ROY, the acrylate group of the polymer interferes with the amine-cyano hydrogen bond unique to the Y polymorph (not found in other forms), and as such facilitates crystallization of the R polymorph.

Following from the discussion above, the templating effect of the microgels alone is expected to bias the polymorph selectivity toward R at lower *M* and Y at higher *M*. We indeed observed continuous nucleation acceleration of form Y with the increase in *M* (Tables 2, 3), although the trend for R still cannot be fully explained in terms of the templating and concentration effects combined. Now we turn our attention to the mesh size effect. We observed the existence of an optimum mesh size for expediting nucleation of R, at which point its frequency of occurrence was maximum. We hypothesize that the optimum mesh size arises from the interplay between polymer–solute interactions and spatial confinement imposed

dx.doi.org/10.1021/ja210006t | J. Am. Chem.Soc. 2012, 134, 673–684

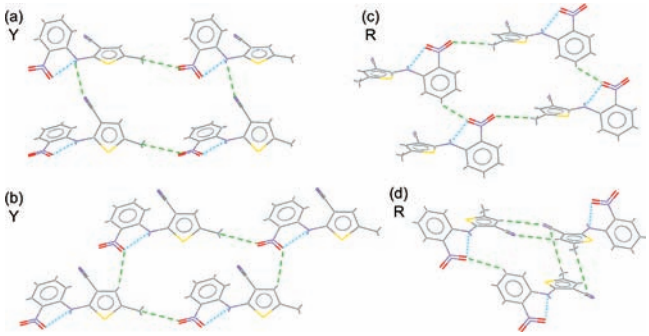

Figure 13. Molecular recognition motifs in ROY crystals of forms Y (a,b) and R (c,d). Green dotted lines denote intermolecular interactions, and cyan dotted lines, intramolecular interactions. Other supermolecular rings can form by different combinations of the same set of intermolecular interactions; however, this figure is not meant to exhaust all the molecular combinations in the ROY crystal, but to illustrate essential intermolecular interactions, which are all depicted here. $\pi-\pi$ stacking is also present in both Y and R forms, exhibiting similar motifs (not shown here).

by the polymer mesh.[20] Specifically, when the mesh size is too small, most of solute molecules are adsorbed to the tightly intertwined polymer chain given the large volume fraction of polymers, thereby reducing the molecular mobility and hindering effective solute–solute interactions essential to nucleus formation (Figure 14a); when the mesh size is too large, a smaller fraction of solute is associated with the polymer, and the nucleation-templating effect of the polymer due to specific polymer–solute interactions is much less significant (Figure 14c); at the optimum mesh size, the polymer–solute and solute–solute interactions are balanced, enabling the solute molecules aligned by adjacent polymer chains to act concertedly in forming the nucleus, given appropriate spacing (Figure 14b). This hypothesis implies that the optimum mesh size should not be the same for polymorphs of the same compound, since their nucleation events are templated by different specific polymer–solute interactions as discussed above, and the spacing required for molecular cooperativity may differ as well. For the ROY system, the separation of optimum mesh sizes between Y and R may be central to the observed favorable polymorph selectivity toward R at M = 575 g/mol, which helps overcome the opposite trend of a templating effect that favors Y with increasing M. As for the CBZ system, the mesh size effect is also evident (Table 1). There exists an optimum mesh size at M = 400 g/mol corresponding to the fastest nucleation rate of form II, whose mass fraction concurrently attained maximum. The polymorph selectivity was maintained at 100% even when M increased beyond its optimum value, probably because the mesh size effect was counterbalanced by the templating and concentration effects, which favored form II at higher M.

In conclusion, we demonstrated polymer microgels are a promising material for controlling crystallization of polymorphs. PEGDA microgels selectively induced nucleation of form II of CBZ, while concomitant crystallization of forms I and II was observed from bulk. In another example, the microgels improved ROY polymorph selectivity toward form R by up to 20 times, whereas bulk crystallization predominantly produced Y or ON depending on the supersaturation. Through these examples, the polymer gels show ability to take the polymorphic system into occurrence domains not accessible through conventional methods. Furthermore, our mechanistic investigations imply that the nucleation-templating effect and the spatial confinement imposed by the polymer network may hold the key to achieving polymorph selectivity. With this insight, selective crystallization of a desired polymorph could be achieved by designing selective polymer chemistry and microstructure. Of course, in order to make this design rational, a detailed molecular understanding of the key reaction coordinates for nucleation processes would be necessary. This work is ongoing in our group, albeit on simpler systems. Our results also help advance the fundamental understanding on crystallization of polymorphs at complex interfaces, in particular, under confined environments.

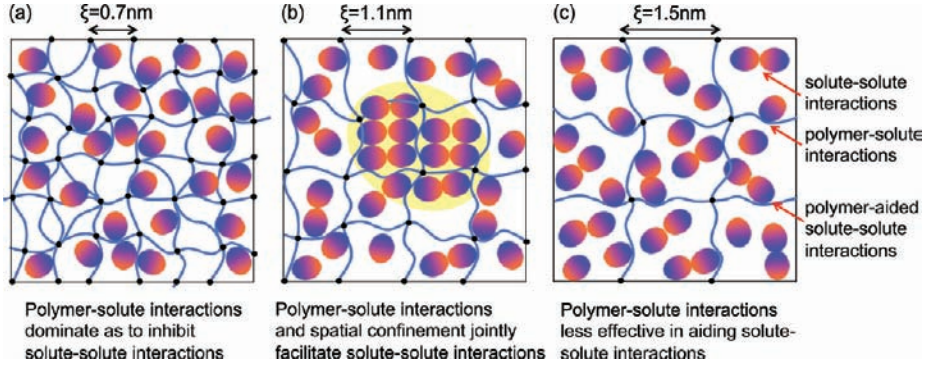

Figure 14. Schematic illustrating the mesh size effect on nucleation. Blue lines denote the polymer mesh with cross-linking points colored black. The polymer mesh drawn here does not necessarily represent the actual physical model but is sufficient to illustrate the role of varying confinement size. Solute molecules are signified with ellipsoids with one end colored blue, which interacts preferentially with the polymer chain, and the other end colored red which is responsible for self-interactions. One example of such molecules is CBZ, with the blue end corresponding to the vinyl group on the azepine ring that interacts with the PEG subchain, and the red end corresponding to the carboxamide group, which dimerizes in CBZ crystals. The molar ratios of solute to monomer units constituting the polymer are drawn to scale, which are calculated from CBZ-partitioning experiments. The size of the solute relative to the mesh size is also drawn to scale approximately for the CBZ system. The relative fraction of solute molecules adsorbed to the polymer chain is estimated by assuming that the number of solute binding sites scales linearly with the PEG subchain length. The optimum mesh size for CBZ nucleation was found to be 1.1 nm (Table 1). Therefore, the nucleus formation is illustrated in (b) as highlighted with yellow background.

dx.doi.org/10.1021/ja210006t | J. Am. Chem.Soc. 2012, 134, 673–684

EXPERIMENTAL METHODS

Materials. Poly(ethylene glycol) diacrylate with average molecular weights of M = 200, 400, 575, and 700 g/mol and tri(ethylene glycol) diacrylate (M = 130 g/mol), poly(ethylene glycol) with M = 200 g/mol (PEG_{200}), 2-hydroxy-2-methyl-1-phenyl-propan-1-one (DC1173) photoinitiator, and Tween20 nonionic surfactant were purchased from Sigma Aldrich Chemical Co. and used as received with no further purification. Deionized water (18.3 MΩ) was obtained using a Millipore Milli-Q purification system. For PEGDA microgel precursors, solutions containing 25% PEGDA, 25% PEG_{200}, and 5% DC1173 by volume in ethanol were prepared for each of the values of the molecular weight M used. Carbamazepine was purchased from Sigma Aldrich (form III), and ROY (form ON) is a gift from Eli Lilly, both used without further purification.

Microgel Synthesis and Characterization. Methods for PEGDA microgel synthesis and microstructure characterization via swelling measurements were described in detail in our previous work (ref 20). In brief, cuboid microgel particles were synthesized by stop-flow lithography (SFL).[23] Microfluidic channels with straight, rectangular cross sections (width = 300 μm, height = 30 μm) were prepared by Soft Lithography. The inlet channel was loaded with a hydrogel precursor using a pressure-controlled manifold. The mask was placed in the field-stop of the microscope, and square features were projected on the precursor by ultraviolet (UV) exposure from a Lumen 200 lamp (Prior) through a wide excitation UV filter set (11000v2: UV, Chroma) when the flow of precursor was stopped. The ultimate feature sizes of the patterned squares were 30 μm × 30 μm, determined through fluorescence imaging of the microchannel during UV illumination. Particles were collected through the outlet channel into a microcentrifuge tube reservoir containing 0.2% v/v Tween20 in a mixture of 62/38 water/ethanol (v/v). Tween20 was added to the outlet reservoir in order to render the microgels colloidally stable during purification. The particles were washed with 62/38 water/ethanol (v/v) several times to remove unreacted species. The particles were solvent-exchanged into pure ethanol while maintaining the original particle concentration, right before being used in crystallization experiments. The apparent average mesh size ξ was estimated using the Flory–Rehner theory by measuring the swelling of the polymer microgel in the crystallization medium relative to the as-synthesized state.

Nucleation Induction Time Distribution. Crystallization measurements of CBZ from ethanol in the presence of PEGDA microgels of various mesh sizes were conducted in an RS10 Clarity Station (Thermo Fisher Scientific). We found that CBZ crystallization is quite sensitive to experimental conditions such as solid impurity concentration, solution water content, stirring speed, etc. Specifically, unfiltered, unstirred CBZ–ethanol solution (S = 2.8, T = 3 °C, solution volume V = 2 mL) tends to yield the stable form III or mixtures of forms III and II, whereas the same solution filtered with 0.2-μm pore size PTFE filters predominantly crystallizes form II. The presence of trace amounts of water in ethanol solution was also observed to inhibit CBZ crystallization. Therefore, absolute, anhydrous ethanol was employed for all crystallization studies to avoid the interference from water. All solutions used in the nucleation induction time study were filtered with 0.2-μm PTFE syringe filters. All procedures involving exposing solution to the air were conducted under the Bio-Safety Cabinet so as to reduce the chance of contamination with unknown impurities, which could affect induction time results.

Around 1000 microgel particles were dispersed in 2 mL of a 34 mg/mL CBZ solution in anhydrous ethanol and were kept suspended by stirring the solution at 300 rpm. Microgels were fully swollen in solution within seconds, which was much shorter than the typical average nucleation induction time. Before crystallization experiments, control experiments were first carried out where the microgels were dispersed in solvent ethanol and kept under the same conditions as used in crystallization experiments. The microgels were sampled at intervals and inspected under the optical microscope to make sure that no significant degradation or aggregation occurred during the course of experiments. In a typical crystallization experiment, 10 samples were loaded into the Clarity station at once. All samples were heated to 42 °C at 5 °C/min to erase the thermo history of the solution, which was previously found to affect the nucleation induction time. After being kept at 42 °C for 30 min, the solutions were cooled at 5 °C/min to 25 °C to generate a supersaturation of 1.63 (defined as the ratio of the starting molar concentration to the saturation molar concentration at the crystallization temperature). This supersaturation level is relative to CBZ form III. The onset of crystallization was signaled by the sudden drop in IR transmission signal through the solution. The time taken from the moment the desired supersaturation was achieved to the moment the IR signal dropped was taken to be the nucleation induction time. Ten samples were cycled 5–10 times between 42 and 25 °C to yield the induction time probability distribution. Toward the end of each heating cycle for dissolving the pre-existing crystals, the solution was inspected under the optical microscope to make sure the microgels were neither aggregated nor degraded. For ROY, the same procedures were followed with 12 mg/mL ROY solutions in anhydrous ethanol. Isothermal crystallization experiments were conducted at 21 °C to achieve a supersaturation of around 2.7 with respect to form R.

For both systems, it is important to eliminate the headspace in the HPLC vial used for crystallization experiments by filling it up with the crystallization solution. This is because, when there is sufficient headspace above the solution, crystals were observed a few millimeters above the solution–glass–air contact line, much before the onset of nucleation in the solution, which may potentially cause unintentional seeding in the solution phase. This phenomenon is probably due to the nucleation from the solution film wetting the glass wall above the solution due to evaporation of the volatile ethanol.

After crystallization, the crystals were collected via filtration for XRD analysis and were examined via optical microscopy (Carl Zeiss Axio Observer).

Quantification of the Polymorph Composition. The polymorph compositions of CBZ crystals were quantified for understanding the concentration effects on the polymorphic outcome. Starting concentrations of 30, 34, 40, 54.2, 80, 120, 141.6 mg/mL of CBZ in anhydrous ethanol were tested in bulk crystallization experiments. All experimental conditions were kept the same as those used in the CBZ nucleation induction time measurements, except for the starting concentration and the temperature set points during the heating cycle for dissolving pre-existing crystals. As soon as crystallization ensued, the CBZ crystals were harvested by passing the slurry through a paper filter, placed in the 0.5-mm deep well machined on a zero background plate and subsequently analyzed using a PANalytical X'Pert PRO Theta/Theta Powder X-ray Diffraction System with Cu tube and X'Celerator high-speed detector. Crystalline powders collected in this manner were analyzed without grinding to avoid polymorph transformation during this process. Although CBZ crystallized as needles, preferred orientation was not a concern even without grinding since the powder mixture comprised very fine crystallites due to vigorous stirring during crystallization and the crystals were collected at the initial stage of crystal growth. All samples analyzed from bulk experiments were mixtures of forms I and II.

The mass fraction of form I, η, was calculated following

$$\eta = k\frac{I(\theta_I)}{I(\theta_I) + I(\theta_{II})} \quad (1)$$

where I denotes relative peak intensity, and θ_I and θ_{II} are the characteristic peak positions (2θ in Figure 2) for forms I and II, respectively. In this case, θ_I = 12.345° and θ_{II} = 5.046°, both being the most intense peaks among the characteristic peaks of their respective phases. Coefficient k is determined experimentally, which converts the peak intensity fraction to the polymorph mass fraction. A calibration curve was made to determine k using CBZ crystal mixtures of known mass fractions of forms I and II. For this purpose, pure forms I and II powders were prepared. Form I crystals were converted by keeping form III crystals at 150 °C in an oven for 4 h. The crystals were taken out of the oven to enable fast cooling to room temperature, which

dx.doi.org/10.1021/ja210006t | J. Am. Chem.Soc. 2012, 134, 673–684

'locks' the polymorph in the metastable form I state. Form II crystals were obtained from solution crystallization induced by a minimal amount of PEGDA microgels with M = 400−700 g/mol. Form I and II powders were mixed to yield five samples with form I mass fractions of 0, 0.20, 0.51, 0.67, 0.75, 1. In the subsequent XRD measurements, the X-ray irradiated length and mask size were set to cover the whole sample area, so that the peak relative intensities thus obtained are not dependent on the mixing uniformity of the forms I and II powders. The linear regression results following eq 1 yielded k = 1.16, R^2 = 0.98.

Polymorph Frequency of Occurrence. For the ROY system, the polymorph frequency of occurrence was quantified instead of the polymorphic composition. This is because the ROY crystals we harvested from one sample vial as soon as crystallization was detected by IR were almost always a single polymorph, not a mixture of several polymorphs. This observation was verified via XRD and optical microscopy. To evaluate the ROY concentration effect on the polymorph frequency of occurrence, bulk crystallization experiments were performed at starting ROY concentrations of 12, 15, and 18 mg/mL, with all other experimental conditions kept the same as used in the induction time study. At each starting concentration, 25−50 samples were tested, examined via XRD and optical microscopy. The polymorph frequency of occurrence was calculated as the percentage of samples crystallized in a particular form out of the total number of samples tested.

Partition Coefficient Measurements. Partition coefficients of CBZ and ROY in PEGDA gels from the bulk solution were determined. A series of gels with varying mesh sizes of approximately 5 mm in diameter and 0.5 mm in thickness were synthesized via UV polymerization following the same formula as used in the microgel synthesis. The residue solvent, porogen, and monomer molecules were removed by washing the gels three times with solvent ethanol, with each wash lasting 12 h to allow enough time for unreacted species to diffuse out of the gels. The gels were subsequently vacuum-dried for 30 min and weighed one by one to obtain the dry gel mass. Each dry gel was then immersed in an excess volume (20 mL) of filtered 34 mg/mL CBZ−ethanol solution at 25 °C for overnight. After equilibrium swelling was reached, the swollen gel was pad dried, weighed, and dropped into an excess volume of ethanol (20 mL) to release CBZ. The total mass of CBZ released was determined by measuring its concentration in ethanol after equilibrating for 24 h, with UV−vis spectroscopy. The absorbance at 285 nm was recorded for quantitative analysis. The CBZ partition coefficient was calculated as the ratio of CBZ mass fraction in solution absorbed by the gel to that in bulk solution. The partition coefficient of ROY was determined by the same method. The gels were immersed in filtered 12 mg/mL ROY solution at 25 °C for overnight. The swollen gels were immersed in excess ethanol to release ROY. Its concentration was determined by measuring the UV absorbance at 397 nm. Three to four independent repeats were carried out for each type of sample to obtain the standard error of the partition coefficient.

Crystal Preferred Orientation. Polymer films of various PEG molecular weights were synthesized via UV polymerization using prepolymer mixtures of the same formulations as used for microgel synthesis, but without adding solvent ethanol and porogen PEG200. Thirty microliters of prepolymer mixture was sandwiched between a glass slide and a quartz slide, both 75 mm × 25 mm in size. The glass slide was silanized with vinyl trichlorosilane, which copolymerizes with the monomer to graft the polymer film to the glass substrate via covalent bonds. The quartz slide was used as a template to make polymer films with minimum surface roughness as possible. The sandwiched prepolymer mixture was subjected to 70 mW/cm^2 UV light for 5 min to complete the polymerization, with the whole sample area irradiated fairly uniformly in the 5000-EC UV Curing Flood Lamp (Dymax Corporation). The quartz slide was subsequently lifted to leave the flat and smooth polymer film conformed to the glass substrate. After synthesis, the polymer films were immersed vertically in 20 mg/mL CBZ−ethanol solution or 10 mg/mL ROY−ethanol solution, which was filtered with a 0.45 μm PTFE membrane syringe filter before adding the polymer films. The solution was then sealed, cooled from 25 to 3 °C, and inspected visually every hour. Once crystals were spotted, the polymer film was withdrawn from the solution to terminate crystallization and immediately dipped into a D.I. water tank vertically to remove loosely attached crystals from the bulk solution (CBZ and ROY are essentially insoluble in water at 3 °C). Almost all crystals were found attached to the polymer films conformed to the glass substrate, whereas the back side of the glass had almost no crystals attached. Bulk crystals were obtained under the same conditions and served as the control sample for XRD analysis.

The specific crystal planes grown from the polymer film were analyzed with XRD in the Bragg−Brentano configuration. The polymer film on the glass substrate was mounted horizontally onto the flat stage. A sample area of 20 mm × 20 mm was irradiated with X-rays in one scan using a programmable divergence slit with 20-mm irradiated length and a 20-mm mask to ensure enough crystals on the polymer film were sampled to yield the statistically representative preferred orientation. Three scans were performed with one polymer film to cover almost the entire surface area. Since only the diffraction from the crystal plane parallel to the polymer film surface was seen by the X-ray detector, the peak that was significantly more intense relative to that of randomly oriented bulk crystals corresponded to the preferred nucleation face induced by the polymer.

Analysis of the XRD data was carried out by normalizing the measured peak intensities I_p^i with the reference peak intensities I_{bulk}^i from the bulk sample, following the formula

$$\eta_i = \frac{I_p^i / I_{bulk}^i}{\sum_i (I_p^i / I_{bulk}^i)} \times 100 \qquad (2)$$

where η_i is the percentage of crystals in orientation i, and p is short for polymer.

AUTHOR INFORMATION

Corresponding Author
trout@mit.edu

ACKNOWLEDGMENTS

We acknowledge the Novartis-MIT Continuous Manufacturing Center for financial support. We are very grateful to Dr. Richard Sear from the University of Surrey for bringing to our attention the quenched disorder phenomenon from the perspective of statistical physics. His research and insightful comments played a key role in deepening our understanding of microgel-induced nucleation.

REFERENCES

(1) Bernstein, J. *Polymorphism in Molecular Crystals*; Oxford University Press: New York, 2002.
(2) Rodriguez-Hornedo, N. *J. Pharm. Sci.* **1999**, *88*, 651−660.
(3) Davey, R. J.; Allen, N.; Blagden, N.; Cross, W. I.; Lieberman, H. F.; Quayle, M. J.; Righini, S.; Seton, L.; Tiddy, G. J. T. *CrystEngComm* **2002**, *4*, 257−264.
(4) Chen, S. A.; Xi, H. M.; Yu, L. *J. Am. Chem. Soc.* **2005**, *127*, 17439−17444.
(5) Desgranges, C.; Delhommelle, J. *J. Am. Chem. Soc.* **2006**, *128*, 15104−15105.
(6) Bernstein, J. *Cryst. Growth Des.* **2011**, *11*, 632−650.
(7) Debenedetti, P. G. *Metastable Liquids: Concepts and Principles*; Princeton University Press: Princeton, NJ, 1996.
(8) Bernstein, J.; Davey, R. J.; Henck, J. O. *Angew. Chem., Int. Ed.* **1999**, *38*, 3441−3461.
(9) Ward, M. D. *Chem. Rev.* **2001**, *101*, 1697−1725.
(10) Hiremath, R.; Basile, J. A.; Varney, S. W.; Swift, J. A. *J. Am. Chem. Soc.* **2005**, *127*, 18321−18327.
(11) Briseno, A. L.; et al. *J. Am. Chem. Soc.* **2005**, *127*, 12164−12165.
(12) Singh, A.; Lee, I. S.; Myerson, A. S. *Cryst. Growth Des.* **2009**, *9*, 1182−1185.

(13) Price, C. P.; Grzesiak, A. L.; Matzger, A. J. *J. Am. Chem. Soc.* **2005**, *127*, 5512−5517.
(14) Olmsted, B. K.; Ward, M. D. *CrystEngComm* **2011**, *13*, 1070−1073.
(15) Ha, J. M.; Wolf, J. H.; Hillmyer, M. A.; Ward, M. D. *J. Am. Chem. Soc.* **2004**, *126*, 3382−3383.
(16) Ha, J. M.; Hamilton, B. D.; Hillmyer, M. A.; Ward, M. D. *Cryst. Growth Des.* **2009**, *9*, 4766−4777.
(17) Beiner, M.; Rengarajan, G. T.; Pankaj, S.; Enke, D.; Steinhart, M. *Nano Lett.* **2007**, *7*, 1381−1385.
(18) Allen, K.; Davey, R. J.; Ferrari, E.; Towler, C.; Tiddy, G. J.; Jones, M. O.; Pritchard, R. G. *Cryst. Growth Des.* **2002**, *2*, 523−527.
(19) Nicholson, C. E.; Chen, C.; Mendis, B.; Cooper, S. J. *Cryst. Growth Des.* **2011**, *11*, 363−366.
(20) Diao, Y.; Helgeson, M. E.; Myerson, A. S.; Hatton, T. A.; Doyle, P. S.; Trout, B. L. *J. Am. Chem. Soc.* **2011**, *133*, 3756−3759.
(21) Canal, T.; Peppas, N. A. *J. Biomed. Mater. Res.* **1989**, *23*, 1183−1193.
(22) Diao, Y.; Helgeson, M.; Siam, Z.; Doyle, P.; Myerson, A.; Hatton, A.; Trout, B. *Cryst. Growth Des.* **2012**, DOI: 10.1021/cg201434r.
(23) Dendukuri, D.; Gu, S. S.; Pregibon, D. C.; Hatton, T. A.; Doyle, P. S. *Lab Chip* **2007**, *7*, 818−828.
(24) Peppas, N. A.; Hilt, J. Z.; Khademhosseini, A.; Langer, R. *Adv. Mater.* **2006**, *18*, 1345−1360.
(25) Grzesiak, A. L.; Lang, M. D.; Kim, K.; Matzger, A. J. *J. Pharm. Sci.* **2003**, *92*, 2260−2271.
(26) Yu, L. *Acc. Chem. Res.* **2010**, *43*, 1257−1266.
(27) Kelly, R. C.; Rodriguez-Hornedo, N. *Org. Process Res. Dev.* **2009**, *13*, 1291−1300.
(28) Lang, M. D.; Kampf, J. W.; Matzger, A. J. *J. Pharm. Sci.* **2002**, *91*, 1186−1190.
(29) Yu, L.; Stephenson, G. A.; Mitchell, C. A.; Bunnell, C. A.; Snorek, S. V.; Bowyer, J. J.; Borchardt, T. B.; Stowell, J. G.; Byrn, S. R. *J. Am. Chem. Soc.* **2000**, *122*, 585−591.
(30) Hilden, J. L.; Reyes, C. E.; Kelm, M. J.; Tan, J. S.; Stowell, J. G.; Morris, K. R. *Cryst. Growth Des.* **2003**, *3*, 921−926.
(31) Nokhodchi, A.; Bolourtchian, N.; Dinarvand, R. *J. Cryst. Growth* **2005**, *274*, 573−584.
(32) Getsoian, A.; Lodaya, R. M.; Blackburn, A. C. *Int. J. Pharm.* **2008**, *348*, 3−9.
(33) Diao, Y.; Myerson, A. S.; Hatton, T. A.; Trout, B. L. *Langmuir* **2011**, *27*, 5324−5334.
(34) Santiso, E. E.; Trout, B. L. *J. Chem. Phys.* **2011**, *134*, 064109.
(35) Shah, M.; Santiso, E. E.; Trout, B. L. *J. Phys. Chem. B* **2011**, *115*, 10400−10412.
(36) Sear, R. *Phys. Rev. E* **2004**, *70*, 021605.
(37) Aizenberg, J.; Black, A. J.; Whitesides, G. M. *Nature* **1999**, *398*, 495−498.
(38) Steiner, T. *Chem. Commun.* **1997**, 727−734.
(39) Ideally, each polymorph should be analyzed separately to obtain their average induction times. However, such an analysis requires additional assumptions to be introduced. The most important assumption (or estimation) is the expected fraction of samples to crystallize as a particular polymorph. Such information is not obtained experimentally since, within the experimental time frame, not all the samples will crystallize, which is dictated by the statistical nature of nucleation. Without this information, the probability $P(t)$ cannot be calculated separately for each polymorph. Alternatively, the whole data set was fitted using a multiexponential model, with each exponential representing the nucleation kinetics of each polymorph. This approach not only yields the average nucleation induction time for each polymorph, it also gives the expected fraction of samples to crystallize in each polymorph, which is represented by the pre-exponential factor a or b (Table 3). The values of fitted parameters a and b are consistent with the experimental observation, since both are no smaller than the observed fraction of samples crystallized in the corresponding polymorph.
(40) Alvarez, A. J.; Singh, A.; Myerson, A. S. *Cryst. Growth Des.* **2009**, *9*, 4181−4188.